

How a β -D-Glucoside Side Chain Enhances Binding Affinity to Thrombin of Inhibitors Bearing 2-Chlorothiophene as P1 Moiety: Crystallography, Fragment Deconstruction Study, and Evaluation of Antithrombotic Properties

Benny D. Belviso,[†] Rocco Caliandro,[†] Modesto de Candia,[‡] Giorgia Zaetta,[‡] Gianfranco Lopopolo,^{‡,||} Francesca Incampo,[§] Mario Colucci,[§] and Cosimo D. Altomare^{*,‡}

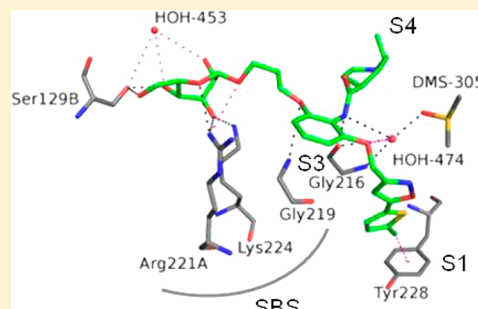
[†]Institute of Crystallography, Consiglio Nazionale delle Ricerche, Via Amendola 122/o, 70126 Bari, Italy

[‡]Department of Pharmacy—Drug Sciences, University of Bari “Aldo Moro”, Via E. Orabona 4, 70125 Bari, Italy

[§]Department of Biomedical Sciences and Human Oncology, University of Bari “Aldo Moro”, Piazza Giulio Cesare 11, 70124 Bari, Italy

S Supporting Information

ABSTRACT: The β -D-glucose-containing compound **3**, bearing 2-chlorothiophene and 1-isopropylpiperidine moieties as binders of the S1 and S4 pockets, respectively, proved to be potent competitive inhibitor of factor Xa (fXa, $K_i = 0.090$ nM) and thrombin (fIIa, $K_i = 100$ nM). The potency of **3** increases, over the parent compound **1**, against fIIa (110-fold), much more than against fXa (7-fold). Experimental deconstruction of **3** into smaller fragments revealed a binding cooperativity of the P3/P4 and propylene-linked β -D-glucose fragments, stronger in fIIa (15.5 kJ·mol⁻¹) than in fXa (2.8 kJ·mol⁻¹). The crystal structure of human fIIa in complex with **3** revealed a binding mode including a strong H-bond network between the glucose O1', O3', and O5' and two critical residues, namely R221a and K224, belonging to the Na⁺-binding site which may allosterically perturb the specificity sites. The potential of **3** as antithrombotic agent was supported by its ability to inhibit thrombin generation and to stimulate fibrinolysis at submicromolar concentration.



INTRODUCTION

Currently, the management of anticoagulation prophylaxis and therapy can benefit from a number of new orally active anticoagulants (NOACs), which have recently become available as alternatives to warfarin and other vitamin K antagonists (VKAs).¹ The NOACs currently approved are dabigatran, available as etexilate prodrug (Pradaxa), which acts as inhibitor of both free and fibrin-bound thrombin (fIIa), and apixaban (Eliquis) and rivaroxaban (Xarelto), which are factor Xa (fXa)-selective reversible inhibitors.^{2,3} Indications of NOACs include stroke prevention in patients with nonvalvular atrial fibrillation (AF) and following hip or knee replacement surgery. Rivaroxaban is also indicated for acute treatment and secondary deep venous thrombosis (DVT) and pulmonary embolism.⁴ The NOACs proved able to overcome a number of shortcomings often associated with the anticoagulant treatment with VKAs. They have more stable and predictable pharmacokinetics, no or fewer interactions with food and drugs, and more importantly, they can be administered in standard doses without the need for laboratory monitoring for dose adjustment. However, the NOACs are not indicated for conditions such as prosthetic heart valve replacement, hemodynamically significant valve disease, and severe renal

failure or impaired liver disease. In addition, they have to be used with caution in patients with renal impairment.⁵

In the past two decades, the rational design of orally bioavailable small-molecule fIIa and fXa direct inhibitors has been intensively supported by X-ray of ligand–protein crystal structures, molecular modeling, and 3D-QSAR approaches,^{6,7} which has allowed achievement of high inhibitory potency. However, despite the large number of discovered potent compounds, only three NOACs are clinically available and a few others are in clinical trials.

We recently reported several *N*-(2- or 3-methoxyphenyl)-piperidine-4-carboxamide derivatives, which selectively inhibit factor Xa^{8,9} or thrombin (fIIa)¹⁰ depending upon the moieties they bear as binders of the specificity enzymes' subsites S1–S4. In particular, compound **1** (Figure 1), bearing 5-chlorothiophen-2-yl and 1-isopropylpiperidin-4-yl moieties as S1 and S4 binders, respectively, proved to be a very potent fXa inhibitor, with high selectivity over fIIa and other serine proteases and good anticoagulant in vitro and ex vivo.^{10,11}

Received: July 17, 2014

Published: September 30, 2014

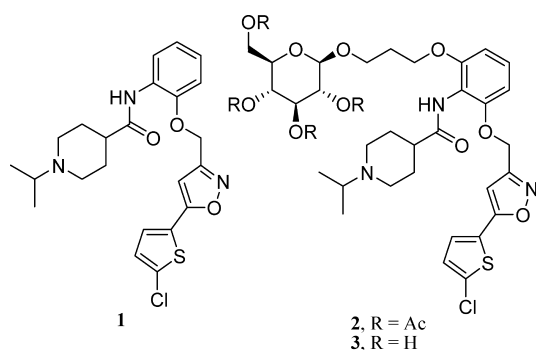


Figure 1. Chemical structures of recently reported potent and selective factor Xa inhibitors, showing *in vitro* and *ex vivo* anticoagulant activity.¹²

According to our docking calculations and in good agreement with the X-ray crystal structures of fXa-inhibitor complexes,^{12,13} compound **1** interacts with the fXa binding pocket by directing the 2-chlorothiophene moiety into the S1 subsite, with the chlorine atom pointing toward the center of the Y228 phenyl ring and the protonated *N*¹-isopropyl residue (the tertiary ammonium head) at the center of the S4 aromatic box, wherein it undergoes efficient cation- π interactions and additional C-H $\cdots\pi$ interactions by the isopropyl group with the side chains of F174, Y99, and W215. Interestingly, the modification of compound **1** by connection of a β -D-glucose fragment via a propylene bridge at the *ortho* position of the isonipecotamido moiety on the central phenyl ring led to the O-glucoside **3** (and its peracetylated derivative **2**), which proved to be not only significantly more potent than the parent compound **1** as fXa inhibitor but also a good fIIa inhibitor with inhibition constant in the nanomolar range, showing anticoagulant activity in both *in vitro* and *ex vivo* assays.¹² In other words, the glucosyl conjugates **2** and **3**, while still retaining fXa-selectivity, displayed improved potency against fIIa. To possibly understand this behavior, in this work we report a fragment deconstruction study of compound **3**, aimed at assessing the contributions of its smaller fragments to the free energy of binding to fIIa and fXa and the crystal structures of human thrombin in complex with both two glucose-based compounds **2** and **3**, which provided us with useful information on their binding modes. The antithrombotic potential of these new inhibitors of fXa and fIIa has been also assessed by investigating their effects on thrombin generation and fibrinolysis.

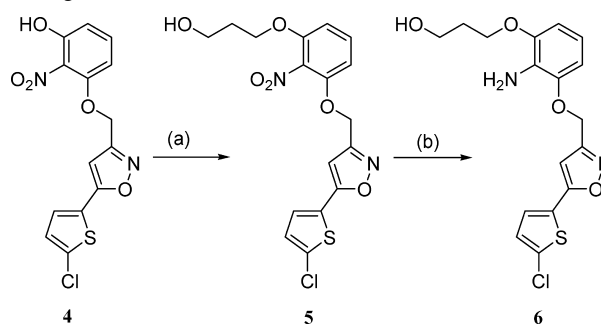
CHEMISTRY

The synthesis of the 5-chlorothiophen-2-yl-bearing compound **6** was accomplished by alkylation of the already reported compound **4**¹² with 3-bromopropanol, followed by reduction of the nitro to amino group using SnCl₂·2H₂O in EtOAc at reflux (Scheme 1).

The synthesis pathways for the molecules containing the 1-isopropylpiperidine P4 fragment and related glucose-bearing derivatives are shown in Scheme 2.

The *N*-isopropyl derivatives **8a,b** were obtained by reductive amination (acetone/Na(CN)BH₃) of the known anilides **7a,b**. Compound **14** was synthesized according to previously reported procedures.¹² The amine derivative **10**, prepared through the reaction between 3-bromopropyl-2,3,4,6-tetra-O-acetyl- β -D-glucose and 2-nitrophenol to afford **9** and subsequent Pd-catalyzed reduction of the nitro group, was coupled

Scheme 1. Synthesis of a 5-Chlorothiophen-2-yl-Containing P1 Fragment Molecule^a.



^aReagents and conditions: (a) 3-bromopropanol, K₂CO₃, Me₂CO, reflux, overnight, 65%; (b) SnCl₂·2H₂O, EtOAc, reflux, 48 h, >95%.

with *N*-Boc-isonipecotic acid using DCC/HOBt as the coupling reagents, followed by the removal of the Boc-protecting group to yield **12**. Reductive amination of **12** with acetone/Na(CN)BH₃ and cleavage of acetyl-protecting groups of **13** with MeONa/MeOH provided compound **14**.

RESULTS AND DISCUSSION

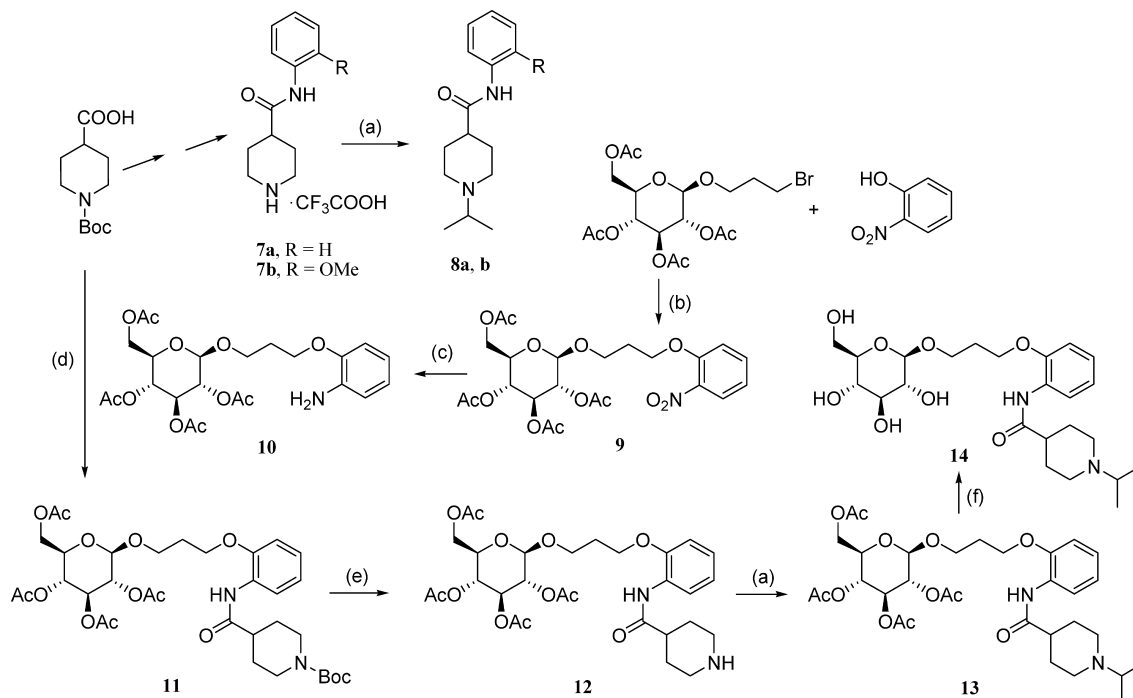
Fragment-Based Structure–Activity Relationships.

The enzymes' inhibition data for fragments and derivatives of the reference molecules **1** and **3**, expressed as inhibition constant (*K*_i) or percent inhibition at 1 mM concentration, are listed in Table 1. The *K*_i values were calculated using the Cheng–Prusoff equation¹⁴ from IC₅₀ values, determined through standard spectrophotometric assays.

Lineweaver–Burk plots, which were generated for the most potent inhibitor **3** (Figure 2) and its parent compound **1**, using fixed amounts of the enzymes and varying concentrations of the substrates in the absence or presence of inhibitor at four different concentrations, showed a competitive inhibition mechanism. A replot of their slopes versus the corresponding inhibitor concentrations provided *K*_i values (fXa, 0.11 ± 0.06 and 0.87 ± 0.18 nM for **1** and **3**, respectively; fIIa, 18 ± 0.45 and 0.096 ± 0.0041 μM for **1** and **3**, respectively), which are close to those assessed by the Cheng–Prusoff equation.

On the basis of the data in Table 1, the β -D-glucose-bearing compound **3**, which is more potent than its peracetylated derivative **2**, inhibits fXa with picomolar potency (*K*_i = 0.090 nM) and fIIa with nanomolar potency (*K*_i = 100 nM), whereas its potency increases, over the parent compound **1**, against fIIa (110-fold) much more than against fXa (7-fold).

Experimental deconstruction of **3** provided us with insights into fXa and fIIa affinity contributions of the 5-(5-chlorothiophen-2-yl)isoxazol-3-yl binding fragment (P1), 1-isopropylpiperidine-4-carboxamide binder (P3/P4), and propylene-linked β -D-glucose fragment (P_G). The data show that all P3/P4-containing fragment molecules [**8a** (R = H), **8b** (R = OMe) and **14**], regardless of whether they bear the hydrophilic P_G group, do not display any noteworthy (>50%) inhibition against both blood coagulation factors at 1 mM concentration, beyond which the determination of IC₅₀ values was prevented because of solubility limits. In contrast, the P1-directed fragment decomposition of **3** resulted in compounds **4a**, **6**, and **6a**, which all showed fIIa/fXa affinity in the micromolar range and a certain preference toward fXa. The glucose-bearing molecule **6a** (fXa *K*_i = 6.9 μM) proved to be 3-fold more potent

Scheme 2. Synthesis of 1-Isopropylpiperidine-Containing P3/P4 Fragment Derivatives^a.

^aReagents and conditions: (a) Na(CN)BH₃, Me₂CO/MeOH, rt, overnight, 50–70%; (b) K₂CO₃, dry DMF, rt, overnight, 70%; (c) H₂ atmosphere, 10% Pd-C, EtOAc, 8 h, 85%; (d) HOBt, DCC, dry DCM, rt, 48 h, 70%; (e) redistilled TFA, DCM, rt, 2 h, 80%; (f) NaOMe, MeOH, rt, overnight, 70%.

Table 1. Factor Xa and Thrombin Inhibition Constants for Fragments and Derivatives of the Reference Molecules 1 and 3

compd	K _i (nM) ^a	
	fXa	fIIa
1 ^b	0.60	11000
2 ^b	0.25	160
3 ^b	0.090	100
4a ^b	11600	31000
6	18300	29800
6a ^b	6900	133000
8a	13% ^c	16% ^c
8b	16% ^c	0% ^c
14	14% ^c	28% ^c

^aInhibition constants, as calculated by the Cheng–Prusoff equation¹⁵ from experimentally determined IC₅₀ values, or % inhibition data at the maximum concentration tested (1 mM) are means of three independent determinations (SEM < 5% of the mean), each performed in duplicate. ^bInhibition data for compounds already reported by us^{10,12} have been redetermined in this study. ^cPercent inhibition for the corresponding compounds at 1 mM concentration.

than the corresponding glucose-lacking compound 6 as fXa inhibitor.

On the basis of the experimental inhibition data, taking 4a as the shortest active molecule encompassing the chlorothiophene S1 binder and the aminophenoxy linker, the P1-directed fragment deconstruction allowed us to assess the contributions, as stepwise relative free energy of binding ($\Delta\Delta G$, kJ·mol⁻¹), to fIIa/fXa affinity of P3/P4 and P_G moieties. The data were analyzed using a double fragment replacement thermodynamic cycle as shown in Figure 3.

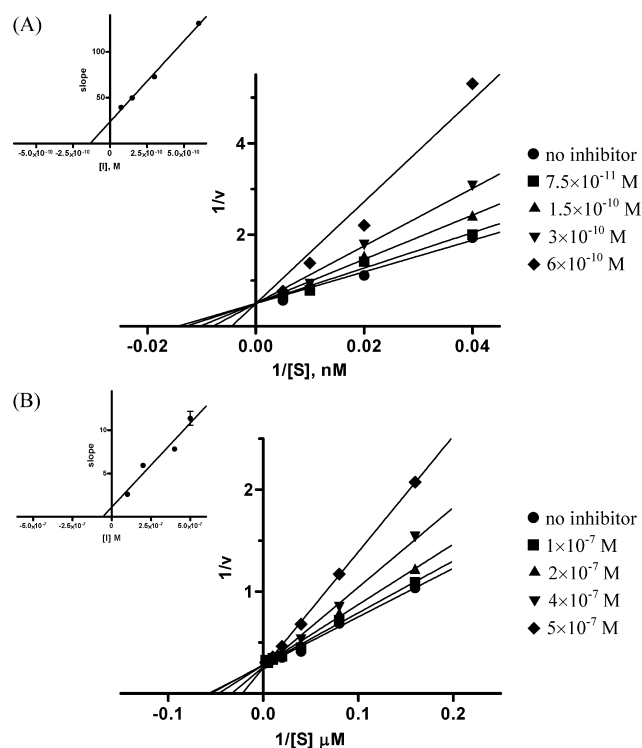


Figure 2. Lineweaver–Burk plots of (A) fXa (2 nM) with the chromogenic substrate S2765, or (B) fIIa (0.45 U·mL⁻¹) with the chromogenic substrate S2238, in the absence or presence of the inhibitor 3; replots of the slopes versus [I] to determine K_i values as the x-axis intercepts are shown in the upper left inserts.

As for fXa, the largest increase in affinity relative to the P1-bearing compounds 4a and 6a resulted from addition of the

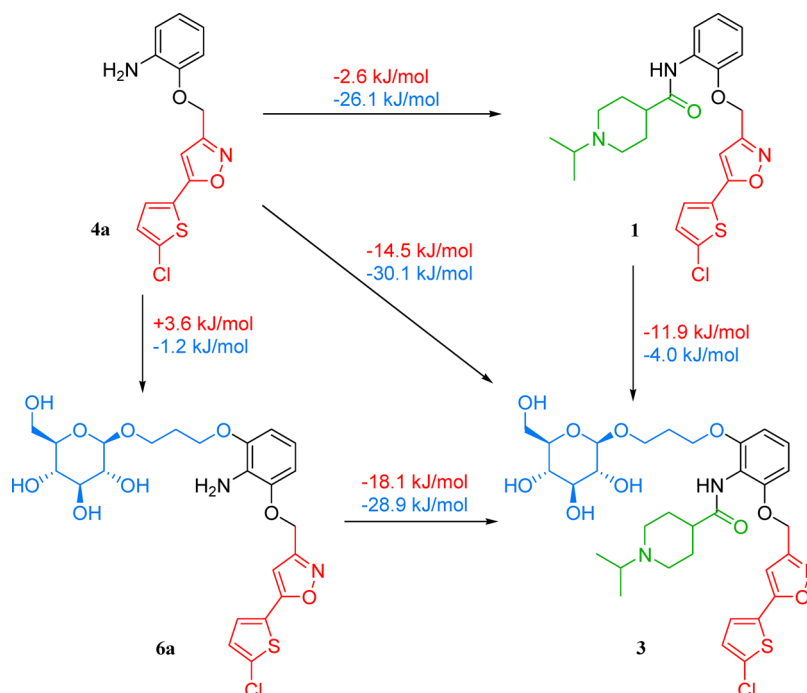


Figure 3. P1-directed fragment deconstruction cycle. $\Delta\Delta G$ values of binding ($\text{kJ}\cdot\text{mol}^{-1}$) are shown on the arrows in red and blue for fIIa and fXa, respectively. Colors of the fragments' structures: P1, red; P3/P4, green; β -D-glucosyl propoxy (P_G), blue. Double fragment replacement cycle reveals a positive cooperative binding between P3/P4 and P_G for both fIIa and fXa inhibition. Such a cooperativity effect is much stronger in fIIa binding ($14.5 - 2.6 + 3.6 = 15.5 \text{ kJ}\cdot\text{mol}^{-1}$) than in fXa binding ($30.1 - 26.1 - 1.2 = 2.8 \text{ kJ}\cdot\text{mol}^{-1}$).

isonipecotamido S3/S4 binder ($\Delta\Delta G_{4a\rightarrow 1} = -26.1 \text{ kJ}\cdot\text{mol}^{-1}$; $\Delta\Delta G_{6a\rightarrow 3} = -28.9 \text{ kJ}\cdot\text{mol}^{-1}$), whereas a small ΔG gain was observed to depend upon the P_G addition (-1.2 and $-4.0 \text{ kJ}\cdot\text{mol}^{-1}$ for $4a \rightarrow 6a$ and $1 \rightarrow 3$, respectively). In contrast, a significant increase in thrombin affinity resulted from the contemporary addition to the minimum active fragment 4a of P3/P4 and P_G ($\Delta\Delta G_{6a\rightarrow 3} = -18.1 \text{ kJ}\cdot\text{mol}^{-1}$; $\Delta\Delta G_{1\rightarrow 3} = -11.9 \text{ kJ}\cdot\text{mol}^{-1}$) and not from the addition of P3/P4 or P_G moieties alone (-2.6 and $+3.6 \text{ kJ}\cdot\text{mol}^{-1}$). Indeed, the $\Delta\Delta G$ “super-additivity” effect of P3/P4 fragment and P_G side chain accounts for a positive cooperativity in both fIIa and fXa, but such a binders' synergistic effect is significantly stronger toward fIIa ($15.5 \text{ kJ}\cdot\text{mol}^{-1}$) than fXa ($2.8 \text{ kJ}\cdot\text{mol}^{-1}$). In other words, the free energy contributions of P3/P4 and P_G to the enzyme binding are almost additive for fXa (small “superadditivity”, less than $3 \text{ kJ}\cdot\text{mol}^{-1}$), whereas the noncovalent interactions attained by these two moieties into the thrombin pockets cooperate to significantly enhance their mutual binding affinity (large “superadditivity”, about $15 \text{ kJ}\cdot\text{mol}^{-1}$).

We measured aqueous solubility, lipophilicity by a reversed phase (RP) HPLC method, and stability both in PBS at physiological pH and human plasma of compounds 1–3 (Table 2). The *O*-glucoside derivative 3 exhibited water solubility (7.33 mM) 14-fold higher than that of the parent compound 1, whereas the peracetylated compound 2 exhibited high lipophilicity and low aqueous solubility ($<1 \mu\text{M}$). All three compounds were stable enough in PBS at pH 7.4 and, with the only exception of the acetate ester derivative 2 ($t_{1/2} = 2.8 \text{ h}$), in human plasma at 37°C up to 4 h incubation (Figure 4).

To understand their binding modes and gain insights into the cooperative binding of the fragments P3/P4 and P_G , the crystal structures of human thrombin in complex with the glucose-based compounds 2 and 3 were solved.

Table 2. Aqueous Solubility, Lipophilicity, and Stability of Compounds 1–3

physicochemical properties	compd		
	1	2	3
aqueous solubility (PBS, pH 7.4) (mM)	0.53	$<1 \times 10^{-3a}$	7.33
$\log k'_w$ ^b	3.49	5.07	3.07
PBS (pH 7.4) half-life (h) ^c	<i>d</i>	<i>d</i>	<i>d</i>
Plasma half-life (h) ^c	<i>d</i>	2.8	<i>d</i>

^aSolubility (mmol L^{-1}) below the detection limit of the quantification HPLC method. ^bLipophilicity parameter as assessed by the logarithm of the polycratic capacity factor determined by a reversed-phase HPLC method (see Experimental Section). ^cStability evaluated in 0.05 M phosphate buffer (pH 7.4, 0.15 M KCl) and human plasma solutions at 37°C . ^dMore than 90% unhydrolyzed compound at 4 h incubation.

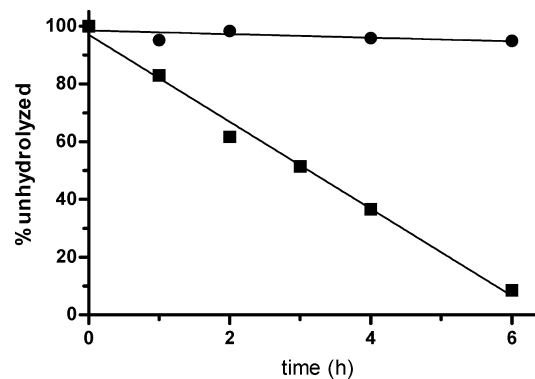


Figure 4. Hydrolysis profile of compound 2 in (●) pH 7.4 PBS (0.15 M KCl) and (■) human serum (first-order half-life 2.8 h)

Crystal Structures of Human Thrombin in Complex with β -D-Glucose-Bearing Inhibitors. The crystals of human

thrombin (*hflIa*) in the presence of the inhibitors **2** and **3** were obtained and structurally solved by X-ray diffraction. Protein/inhibitor adducts were crystallized starting from *hflIa* crystals through the soaking technique; therefore, they preserved the monoclinic unit cell, the space group C2, the molecular arrangement, and the hirugen molecule (used to prevent the autolysis of the protein during the crystallization experiment) in the exosite I of the progenitor *hflIa* crystal.¹⁵ The unit cell and refinement parameters for crystal structures of *hflIa* in complex with **2** (PDB 4NZE) and **3** (PDB 4N3L) are listed in Table 3.

Table 3. Unit Cell and Refinement Parameters for 4NZE (2) and 4N3L (3) Structures^a

	4NZE (2)	4N3L (3)
wavelength (Å)	0.978	1.5418
space group	C2	C2
cell dimensions (Å)		
<i>a</i>	67.460	66.990
<i>b</i>	71.640	71.660
<i>c</i>	71.800	71.790
resolution range (Å)	1.98–37.86	1.94–13.65
unique reflections	22000	24649
completeness (%)	97.8 (97.0)	99.0 (94.0)
<i>I</i> / σ (<i>I</i>)	9.2	6.8
average <i>B</i> -factor (Å ²) (from Wilson plot)	23.2	22.8
average <i>B</i> -factor of inhibitor molecule atoms (Å ²)	65.3	31.8
<i>R</i> (%)	19.9 (24.3)	21.9 (34.0)
<i>R</i> _{free} (%)	24.8 (29.2)	24.6 (36.9)
protein atoms	2536	2580
inhibitor molecule atoms	59	47
DMSO molecules	6	6
water molecules	118	79
RMSD bond lengths (Å)	0.007	0.007
RMSD bond angles (deg)	1.419	1.078

^aData in parentheses refer to the higher resolution shell.

In both crystal structures, the inhibitor molecules are located in the active site of the protein and mainly interact with residues belonging to S1 and S3/S4 sites. The thrombin conformation is not affected by the presence of the inhibitor molecules, as suggested by the low values of root-mean-square deviation (RMSD) of all the C α atoms, calculated between our structures and the one used as the search model for the structure determination process (PDB 1HGT¹⁶), which does not contain active-site inhibitor molecules (RMSD equals 0.38 and 0.54 Å for 4N3L and 4NZE, respectively). Atomic displacements in specific sites are instead observed: (i) the autolysis site of the protein from E146 to K149e (RMSD equals 0.55 and 1.76 Å for 4N3L and 4NZE, respectively) and (ii) the S2 loop from Y60a to W60d (RMSD equals 1.17 and 0.79 Å for 4N3L and 4NZE, respectively). They can be explained taking into account (i) the mobility for the new terminations produced by the autolysis of the protein and (ii) the small variation induced by the presence of a molecule in the thrombin active site on the rigid hydrophobic S2 loop. In addition, the residue E186d shows large RMSD value (1.60 and 1.84 Å for 4N3L and 4NZE, respectively), but notwithstanding the closeness of this residue to the active site, the atomic displacement does not seem to arise from the inhibitor–protein coupling. Despite the presence of two different inhibitor molecules, there were no apparent conformational differences

between the two crystal structures (RMSD equals 0.18 Å). Residues belonging to the active site have RMSD values of 0.9 Å at most, suggesting that the *hflIa* active site does not undergo significant changes because of the presence of the inhibitors **2** and **3**. However, it should be noted that the last result could be biased by the technique used to produce protein–ligand crystals; indeed, protein movements triggered by ligand binding could be hindered by crystal packing in the case of soaking experiments.

Inhibitor Binding Modes to *hflIa*. Figure 5 shows the inhibitors **2** (cyan-colored C atoms) and **3** (green-colored C

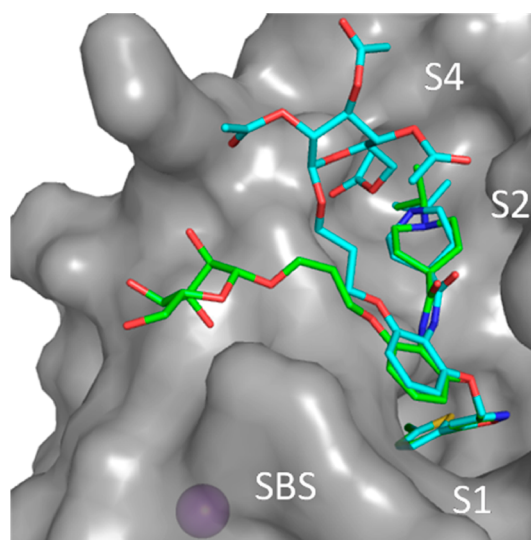


Figure 5. Structures of the inhibitors **2** (C atoms in cyan) and **3** (C atoms in green) in the human α -thrombin binding site after the superimposition of 4NZE and 4N3L X-ray crystal structures. The inhibitor structures are shown in stick representation with O in red and N in blue color (sulfur and chloride atoms are hidden in the S1 pocket). The molecular surface of thrombin in the 4N3L structure is shown in gray. The thrombin binding sites (S1, S2, and S4) for small-molecule direct inhibitors and sodium binding site (Na⁺ as violet sphere from thrombin structure, PDB 2ZFE) are highlighted.

atoms) in the binding site of *hflIa* after the superimposition of the protein crystal structures. The chlorothiophene moieties of the two inhibitors are completely overlapped in the S1 pocket, whereas just small variations occur in the 1-isopropylpiperidine fragments located in S4.

In both cases, the chlorine atom is involved in nonbonded interactions with the phenyl ring of Y228 located on the back wall of S1 (Figure 6). The interactions have a face-on geometry with the Cl atoms distant 3.9 Å from the centroid of the Tyr aromatic ring, in accordance with the results expected for a Cl– π interaction.¹⁶ The amide nitrogen of **2** and **3** forms an extended H-bond network with G216 and a water molecule, which contributes to strengthen the binding of ligand to the protein. In the case of **3** (Figure 6a), the G219-NH forms a H-bond with the ligand ether oxygen connecting the central phenyl linker with the propylene-linked glucose (N–O distance = 3.4 Å).

The main difference between the binding modes of **3** (Figure 6a) and **2** (Figure 6b) resides in the orientation of the propylene-glucose side chains (P_G) into the binding site of *hflIa*. Figure 5 shows that the P_G fragment in **3** lies on the lower part of the access channel to the active site, whereas it tilts and shifts toward S4 and S2 (loop 60) when β -D-glucose is

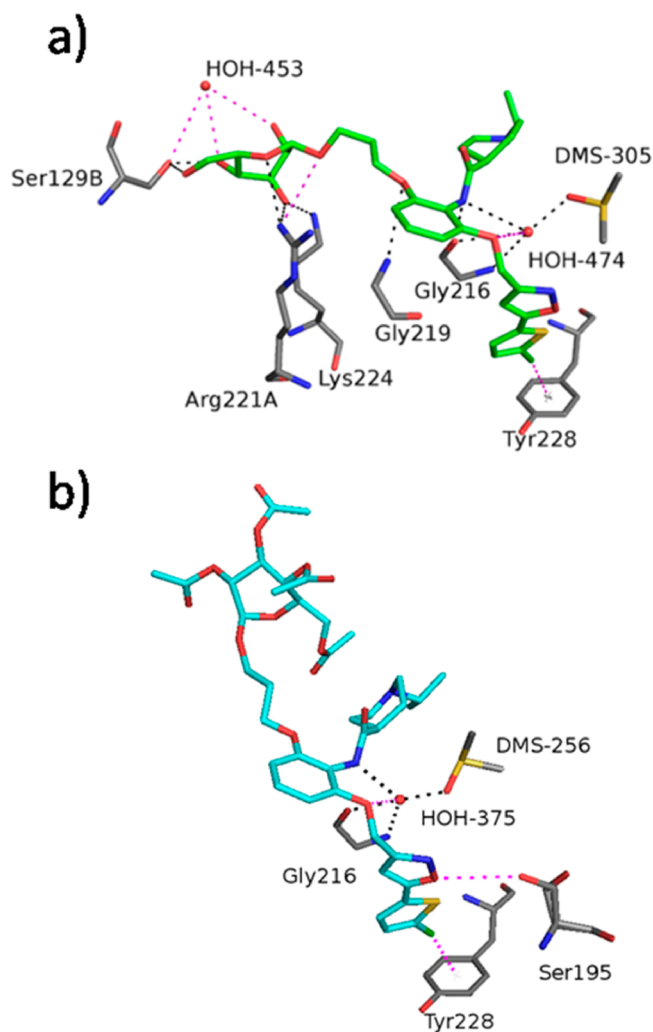


Figure 6. Binding modes of inhibitors 3 (a) and 2 (b) to human α -thrombin as revealed by X-ray crystallography. Compounds 2 and 3 are shown as stick representations with O in red, N in blue, S in yellow, and Cl in dark green color; C atoms are in green and cyan colors for 3 and 2, respectively. Protein residues interacting with ligands are in stick representation with O in red, N in blue, and C in gray. H-bonds with H-donor/H-acceptor distance $< 3.5 \text{ \AA}$ are shown as black dashed lines; weaker H-bonds ($3.5 < \text{H-donor/H-acceptor distance} < 4 \text{ \AA}$) are in magenta dashed lines.

peracetylated as in 2. In the crystal structure of *h*fIIa complexed with 3, the orientation of the P_G fragment is driven by an H-bond network formed between the basic side chains of R221a and K224, which are two important residues involved in the Na⁺ binding site (SBS), and O1', O3', and O5' of the glucose moiety (Figure 6a). In detail, the guanidyl group of R221a makes H-bonds with the glucose O1', O3', and O5', whereas the K224 amino group is H-bonded with O3'. Anchored in the lower part of the access channel to the fIIa active site, the glucose moiety of 3 approaches the S129b side chain of a symmetry-related fIIa molecule, allowing H-bond formation between S129b-O γ , glucose O6', and a water molecule (HOH-453, Figure 6a). Although these H-bonds may be due to a molecular rearrangement of the protein in the crystal of the adduct with compound 3, they provide evidence that only "free" OH groups in the glucose moiety of 3, likely due to a higher density of negative charge compared to the OAc groups in 2, could more easily retrieve H-donor/acceptor groups, such

as S129b-O γ and w453 (Figure 6a), interacting with them to stabilize the enzyme–inhibitor complex. As a matter of fact, the absence of H-bonds involving the peracetylated glucose moiety of 2, along with other factors such as steric repulsion, may prevent interactions with the access channel to the active site by the P_G fragment, which instead is oriented toward the solvent outside the protein close to S2 and S4 (Figure 6b). The stabilization effect of these H-bonds in 2 and 3 can be inferred by examining the refined values of the crystallographic B-factors of their atoms (Figure 7). Atoms having higher B-factors (high vibrational motions) are colored in red, whereas atoms having lower B-factors (low vibrational motions) are colored in blue.

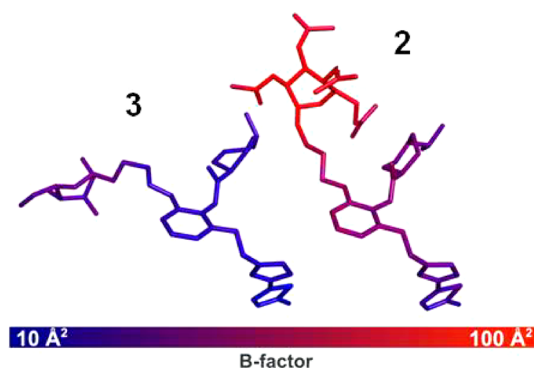


Figure 7. Crystallographic B-factor for inhibitors 2 (right) and 3 (left). Atoms are colored depending on their B-factors: from blue for atoms having lower B-factor values to red for atoms having higher B-factor values.

The largest differences can be observed in the glucose portions (prevailing red in 2, prevailing blue in 3), but significant differences also occur in the remaining part of the two ligand structures; the structure of 3 is prevalently colored in blue, suggesting that the whole molecule is strongly anchored to the protein, whereas the central portion of 2 (encompassing the phenyl linker and the isonipecotamide P3/P4 moiety) is less stable than in compound 3, with effects on the stability of its 5-(5-chlorothiophen-2-yl)isoxazol-3-yl group as the S1 binder. This result suggests that the stabilization effect due to formation of H-bonds with K224 and R221a is not limited to the glucose moiety but affects the stability of binding of the whole ligand structures up to the S1 binding fragment. The effect of stabilization also affects the B-factor of the protein residues close to the two ligands, as shown in Table 4, which summarizes the average B-factors of the amino acid residues and molecules (DMSO, water) closer than 4 \AA to the ligands.

For each residue, the B-factor in 4N3L (3) is lower than that in 4NZE (2), highlighting that the binding interactions in 4N3L are more stable than in 4NZE. The B-factors relating to DMSO (DMS305 and 256 for 4N3L and 4NZE, respectively) and water molecules (HOH474 and 375 for 4N3L and 4NZE, respectively), which participate to form an H-bond network with the two ligands near the entrance to the S1 pocket (Figure 6), are those mostly affected by the acetylation of the glucose OH groups in the ligand structures, whereas G216 is the residue in close proximity to S3 that shows the larger difference in the B-factor between the 4N3L and 4NZE structures. Significant differences (ca. 10%) also emerge for the residues R221a and W60d belonging to Na⁺ binding loop and the specificity site S2, respectively.

Table 4. Crystallographic B-Factor of the Thrombin Residues and Molecules Closer than 4 Å to the Ligands 2 and 3, Listed in Descending Order of the B-Factor Difference between the Two Crystals^a

molecule/residue	4NZE (2)	4N3L (3)	location/specificity site
DMS	48.49	31.33	DMSO in the active site
HOH	38.51	23.57	water in the active site
Gly216	27.63	16.92	close proximity to S3
Arg221a	38.06	27.71	Na ⁺ binding loop
Trp60d	48.95	38.95	S2 (loop 60)
Glu192	36.04	27.25	close proximity to S1
Glu217	31.72	24.22	close proximity to S3
Gly219	31.72	24.88	Na ⁺ binding loop
Cys191	25.62	18.99	Na ⁺ binding loop
Cys220	28.55	23.25	Na ⁺ binding loop
Leu99	24.99	20.17	close to S2
Val213	14.10	9.58	last β -strand close to Na ⁺ binding loop
Glu97a	42.09	38.13	S4
Lys224	25.66	21.99	Na ⁺ binding loop
Ser195	19.25	15.73	catalytic residue
Ala190	18.22	15.08	S1
Tyr228	12.90	9.94	S1
Trp215	19.82	16.92	S3
Asp189	20.92	18.05	S1
Gly226	15.00	13.06	Na ⁺ binding loop
Ile174	22.84	21.48	S4
Tyr60a	27.11	26.46	S2 (loop 60)

^aLocation and/or specificity site of each residue is shown in the last column.

As mentioned above, R221a and K224, which form a H-bond network with the glucose moiety of 3 (and not with the peracetylated glucose of 2), are two critical residues of the Na⁺ binding loop in thrombin, which is known for allosterically regulating the enzyme catalytic activity (the residues of the catalytic triad are about 20 Å away from the bound Na⁺) and influences its specificity sites.¹⁷ The binding of Na⁺ triggers the transition from slow (anticoagulant) to fast (procoagulant) thrombin forms, affecting thrombin specificity toward a number

of physiological and synthetic ligands. Indeed, the Na⁺-bound fast form is specific toward fibrinogen, the thrombin receptors, thrombomodulin and antithrombin III, whereas the Na⁺-free slow form is specific toward protein C.¹⁸ From the structural point of view, the SBS lies within a cylindrical cavity formed by three antiparallel β -strands of the B chain, diagonally crossed by the sequence E188–E192 and shaped by the loop D221–K224, which connects the last two β -strands. The sequence C220–G226, encompassing the Na⁺-binding loop and part of the last β -strand of the B chain, is almost completely conserved in thrombin from different species.¹⁹ Sodium ion is octahedrally coordinated by the carbonyl O atoms of R221a and K224 and four buried water molecules, and the Na⁺-binding environment is stabilized by three ion pairs, namely R221a···E146 (a residue of the neighbor autolysis loop), K224···E217, and a bidentate ion pair formed by R187 with D221 and D222 flanking R221a. A disulfide bond between C220 and C191 anchors the Na⁺-binding loop to the neighbor sequence 187–192, which includes two critical residues, namely D189 at the bottom of S1 (its side chain is 5 Å away from the bound Na⁺) and E192 in close proximity to S1.²⁰

Actually, a closer examination of the crystal structures 4NZE and 4N3L did not reveal any significant difference in their specificity sites' folding, irrespective of the small-molecule ligand structure, and both structures reproduce the fast form of thrombin, which is overrepresented in PDB. This could be due to the high Na⁺ concentration used in our crystallization experiments. In addition, it should be noted that there are cases in which putative slow forms of thrombin (e.g., 1SGI) are conformationally indistinguishable from the fast forms.²¹ Nonetheless, it is reasonable to assume that multiple and strong H-bond interactions between the P_G fragment of the most potent inhibitor 3 and R221a and K224, and G219 as well, all residues belonging to the Na⁺-binding loop, could allosterically perturb the thrombin specificity sites, especially allowing a closer (more efficient) binding of the S1 and S3/S4 binders of the inhibitors. In the case of binding of 3 to fIIa, it is likely that when the SBS is perturbed through H-bond interactions of the glucose moiety with key residues (i.e., R221a and K224), perturbation at other sites (S1 and S3/S4) reduces their specificity beyond simple additivity of the single

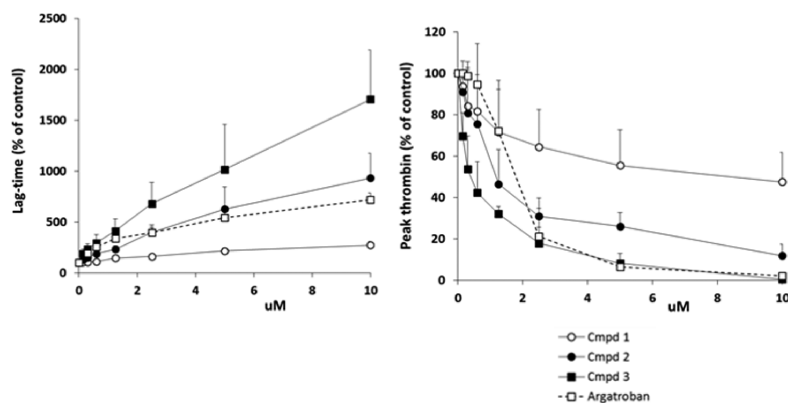


Figure 8. Effect of compounds 1–3 and argatroban on thrombin generation as assessed by the calibrated automated thrombography. Citrated human plasma was spiked with the indicated concentrations of test compounds or vehicle, and clotting was induced by low tissue factor concentration, phospholipids, and calcium (details in Experimental Section). The following parameters of the thrombin generation curves were considered: (i) lag-time (left panel), (ii) peak thrombin concentration (middle panel), and (iii) endogenous thrombin potential (ETP, right panel). Results are expressed as percent of the values recorded in the corresponding control plasma samples supplemented with the vehicle alone. Data are the means \pm SD of three independent measurements carried out on different plasma samples.

perturbations, allowing further stabilization of the interactions with particular residues in these sites (e.g., H-bonds with G216-C=O and G219-NH close to S3). The large and significant superadditivity of free energy contributions of P3/P4 and P_G fragments into compound 3 to thrombin binding (+15.5 kJ·mol⁻¹), which revealed a positive cooperative binding of the inhibitor fragments, is consistent with such a kind of allosteric regulation of the specificity sites.

Anticoagulant Activity. The anticoagulant activity of our most potent fXa/fIIa inhibitors 1–3 was investigated in vitro by measuring their effects on tissue factor-induced thrombin generation (TG). The assay was performed in human plasma, using the calibrated automated thrombography (CAT) as described by Hemker et al.,²² and compared with the direct thrombin inhibitor (DTI) argatroban. The TG assay is considered one of the most relevant tests for assessing the hemostatic function and is one of the most sensitive for monitoring the anticoagulant activity of drugs targeting fXa. At variance with the classical clotting test, such as aPTT (activated partial thromboplastin time) and PT (prothrombin time), the TG assay, thanks to the use of several parameters, each reproducing a distinct phase of the clotting cascade, makes it possible to distinguish between drugs with different mechanisms of action.²³

Pooled citrated human plasma was spiked with 1–3 or argatroban at concentrations of 0.01–10 μM, and the inhibitory potencies of the test compounds were assessed by three CAT parameters: (i) the lag-time (LT) that is the time required to generate the first traces of thrombin, (ii) the thrombin peak (TP), and (iii) the endogenous thrombin potential (ETP), which is a measure of the total thrombin formed (i.e., the area under the TG curve). The concentration-dependent effects of the test compounds on the CAT parameters are shown in Figure 8.

LT was variably prolonged by the three molecules, the β-D-glucose-bearing compound 3 being the most active and 1 the least active. At the highest tested concentration (10 μM), 3 prolonged the lag-time more than 15 times over the control, while 1 and 2 showed about 3-fold and 9-fold LT prolongations, respectively. Compared with argatroban, 2 showed similar behavior, whereas 3 caused a significantly greater delay of thrombin appearance. Fairly similar results were obtained when thrombin peak was considered. Indeed, the strongest inhibition was observed with 3, which caused a 50% reduction at about 0.3 μM, as compared to 1.2 and 10 μM for compounds 2 and 1, respectively. Interestingly, considering the IC₅₀ values, both the glucosyl derivatives 2 and 3 proved to be more potent than argatroban (IC₅₀ 1.9 μM). Concerning the ETP parameter, compound 1 did not induce any appreciable decrease, 2 displayed an intermediate inhibitor activity with IC₅₀ of 10 μM, and 3 was the most active, with IC₅₀ value comparable to that of argatroban (3.4 and 2.4 μM, respectively).

Profibrinolytic Activity. In the past decade, it has become increasingly clear that the enhancement of fibrinolysis is an important component of the antithrombotic activity of anticoagulant drugs.²⁴ Because thrombin has been shown to inhibit fibrinolysis through different mechanisms,²⁵ the profibrinolytic activity of anticoagulants is almost entirely due to their ability to inhibit thrombin formation or activity. However, not all anticoagulants promote fibrinolysis with the same efficiency,²⁵ suggesting that the relationship between inhibition of coagulation and stimulation of fibrinolysis is not

straightforward. For example, the thrombin inhibitors hirudin and PPACK were unable to stimulate fibrinolysis, even at concentrations causing a strong anticoagulant effect.²⁶ Moreover, the synthetic pentasaccharide fondaparinux, an indirect selective fXa inhibitor (its anticoagulant activity is mediated by the high affinity binding to the anticoagulant factor antithrombin III), has been shown to stimulate fibrinolysis at concentrations much higher than achieved in patients.²⁷

The effect of our compounds in an in vitro model of plasma clot lysis is shown in Figure 9. Results are expressed as lysis

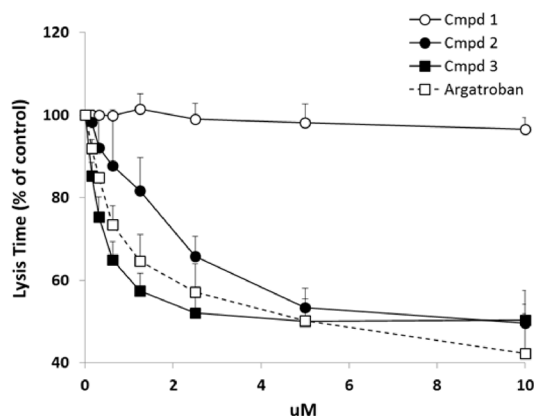


Figure 9. Effect of compounds 1–3 and argatroban on plasma fibrinolysis. Citrated human plasma was spiked with the indicated concentrations of test compounds or vehicle. The lysis time of tissue factor-induced clots supplemented with t-PA was evaluated by a turbidimetric assay (details in Experimental Section). Results are expressed as percent of the lysis time recorded in the same plasma samples supplemented with the vehicle alone. Data are the means ± SD of three independent measurements carried out on different plasma samples.

time, that is, the time needed to lyse the fibrin clot by 50% (the shorter the lysis time the greater the profibrinolytic activity of the compound). In this model, the maximum effect that can be achieved is a reduction of lysis time of 50–60%, which is obtained when the antifibrinolytic effects of thrombin are completely neutralized. Therefore, the EC₅₀ corresponds to the concentration that shortens the lysis time by 25–30%. In reasonable agreement with the ETP results reported above, compound 3 was the most active, with EC₅₀ of 0.3 μM, followed by compound 2, with EC₅₀ of 1.8 μM, and compound 1, which was practically inactive. In this model, the EC₅₀ of argatroban was 0.6 μM.

As a matter of fact, compound 1, which proved a potent and highly selective fXa inhibitor ($K_i = 0.6$ nM), with a low inhibition potency against fIIa ($K_i = 11$ μM), did not show significant effects on TG and fibrinolysis up to the concentration of 10 μM. Its chemical modification, through connection of a propylene-linked β-D-glucose in suitable position of the central phenyl ring, led to the O-glucoside derivative 3, which not only enhanced binding affinity to fXa ($K_i = 0.09$ nM) and fIIa ($K_i = 100$ nM) but also proved able to stimulate fibrinolysis at the same submicromolar concentrations producing the anticoagulant effects assessed by the in vitro TG assay, its efficacy being comparable to that of argatroban, a DTI currently in clinical use. Compound 2, that is, the paracetyl precursor of 3, showed intermediate potency between 1 and 3 on enzymes' inhibition, as well as on anticoagulant and profibrinolytic activities.

CONCLUSIONS

The propylene-linked β -D-glucosyl derivative **3** has been discovered which inhibits fXa and fIIa with different potencies (K_i values equal to 0.090 and 100 nM, respectively). Compared to the parent compound **1**, compound **3**, while remaining a fXa-selective inhibitor, increases its binding affinity to fIIa (110-fold) much more than to fXa (7-fold). Thanks to its unique features, compound **3** is different from the direct fXa inhibitors currently in use in the clinic, i.e., rivaroxaban and apixaban, which display a greater than 10000-fold selectivity for fXa over other human coagulation proteases, including thrombin.^{28,29}

In this study, we virtually decomposed **3** into smaller fragments, synthesized them, and determined their inhibition effects on both fIIa and fXa in order to explore ΔG "superadditivity" of the linked fragments as proof of possible cooperative effects in enzyme–ligand interactions. Our experimental fragment deconstruction study highlighted a long-range binding cooperative effect between the 1-isopropylpiperidine-4-carboxamide S3/S4 binder and the C3-alkyl-linked β -D-glucose fragment, which resulted in stronger fIIa ($15.5 \text{ kJ}\cdot\text{mol}^{-1}$) than fXa ($2.8 \text{ kJ}\cdot\text{mol}^{-1}$), thereby suggesting that the interactions attained by the two fragments can mutually increase in their strength.

The crystal structure of the hfIIa–**3** complex provided a picture of the binding mode of **3**, which includes, besides the expected interactions of the 2-chlorothiophene and 1-isopropylpiperidine moieties with the S1 and S4 pockets, respectively, an H-bond network between the glucose O1', O3', and O5' and the side chains of R221a and K224, which are two key residues belonging to the thrombin SBS. Similar H-bond interactions are not formed when β -D-glucose is peracetylated as in **2**, and the sugar-bearing side chain in fact tilts and shifts toward S4 and S2 (loop 60). It has been established that SBS, depending upon the Na^+ concentration, may allosterically regulate the thrombin catalytic activity, also affecting the specificity sites.¹⁸ It is likely that when SBS is perturbed, due to H-bond interactions between the glucose moiety in **3** and R221a and K224 side chains, it could affect the S1–S3 environments, reducing their specificity for the ligand moieties and/or allowing further stabilization of the interactions with particular residues in these sites (e.g., H-bonds with G216-C=O and G219-NH close to S3). Reasonably, the large "superadditivity" ($+15.5 \text{ kJ}\cdot\text{mol}^{-1}$) of the ΔG contributions to thrombin binding by P3/P4 and P_G fragments suitably placed in compound **3** could reflect the SBS-dependent allosteric regulation of the specificity sites.

On the basis of the TG assay, which is the most pathophysiologically relevant clotting test currently used, we showed that compound **3** has the strongest anticoagulant activity. It prolongs the lag-time and reduces both thrombin peak and ETP with an efficacy comparable to that of the intravenous DTI argatroban. Another major feature of **3** is its ability to markedly stimulate fibrinolysis at the same concentrations producing the anticoagulant effect. In contrast, the parent compound **1**, which showed about 20000-fold selectivity for fXa over thrombin, does not significantly affect both TG and fibrinolysis up to the concentration of $10 \mu\text{M}$.

While the SARs and crystallographic information presented here will be valuable for the design of new efficacious fIIa and fXa inhibitors, compound **3** is worthy of further investigation aimed at better characterizing its potential as antithrombotic agent.

EXPERIMENTAL SECTION

General Methods. Several compounds were synthesized according to known procedures with slight modifications; their melting points and spectral data were in full agreement with those reported in literature, and no effort was made at this stage to optimize the yields. Unless otherwise stated, starting materials, and all chemicals and solvents as well, were purchased from Sigma-Aldrich. Chromatographic separations were performed on silica gel 60 for column chromatography (Merck 70–230 mesh, or alternatively 15–40 mesh for flash chromatography). Melting points were determined by using the capillary method on a Stuart Scientific SMP3 electrothermal apparatus and are uncorrected. IR spectra were recorded using KBr disks on a PerkinElmer Spectrum One FT-IR spectrophotometer (PerkinElmer Ltd., Buckinghamshire, UK), and the most significant absorption bands are listed. ¹H NMR spectra were recorded at 300 MHz on a Varian Mercury 300 instrument. Chemical shifts are expressed in δ and the coupling constants J in hertz (Hz). The following abbreviations are used: s, singlet; d, doublet; dd, doublet–doublet; t, triplet; q, quartet; qt, quintet; m, multiplet. Signals due to NH and OH protons were located by deuterium exchange with D₂O. Mass spectra of final products and intermediates were recorded on an Agilent GC/MS 6890–5973 using electrospray ionization (ESI).

For newly synthesized tested compounds, HRMS data, as a further criterion of compound identity, and combustion analysis, as a criterion of purity ($\geq 95\%$), have been supplied. HRMS were recorded on Agilent 6530 Accurate-Mass Q-TOF LC/MS system (laboratory service of the Consorzio Interuniversitario di Ricerca in Chimica dei Metalli nei Sistemi Biologici, CIRCMSB, Bari, Italy). Elemental analyses (C, H, N) were performed on an Euro EA3000 analyzer (Eurovector, Milan, Italy), and the results agreed to within $\pm 0.40\%$ of the theoretical values. The syntheses of the β -D-glucose-containing compounds **9–14** are described below, whereas experimental details on synthesis, along with analytical and spectral data, of non-glycosylated fragments and intermediates of the reference molecules **1** and **3** (i.e., compounds **5**, **6**, **7a**, **7b**, **8a**, and **8b**) are reported in Supporting Information.

3-(2-Nitrophenoxy)propyl 2,3,4,6-tetra-O-acetyl- β -D-glucopyranoside (9). K_2CO_3 (620 mg, 4.50 mmol) was added to a solution of 2-nitrophenol (300 mg, 2.14 mmol) in dry DMF (10 mL), and the mixture was stirred at room temperature for 30 min. Then, 3-bromopropyl 2,3,4,6-tetra-O-acetyl- β -D-glucopyranoside (1.0 g, 2.14 mmol) dissolved in dry DMF (5 mL) was added, and the reaction mixture was stirred overnight at room temperature, diluted with water (250 mL), and extracted with EtOAc ($3 \times 50 \text{ mL}$). The combined organic layers were sequentially washed with 2 N NaOH ($3 \times 30 \text{ mL}$) and brine (50 mL), dried (Na_2SO_4), filtered, and concentrated under reduced pressure to afford an oil, which was purified by flash chromatography (mobile phase *n*-hexane/EtOAc, 1:1 v/v) to provide **9** as white solid (650 mg, 70% yield), mp 129–131 °C. IR (KBr): 2966, 2917, 1755, 1659, 1521, 1367, 1231, 1166, 1038, 858, 742 cm^{-1} . ¹H NMR (300 MHz, CDCl_3) δ 7.82 (d, $J = 9.0 \text{ Hz}$, 1H), 7.52 (t, $J = 7.5 \text{ Hz}$, 1H), 7.07 (d, $J = 8.0 \text{ Hz}$, 1H), 5.21 (t, $J = 9.0 \text{ Hz}$, 1H), 5.06 (t, $J = 9.0 \text{ Hz}$, 1H), 4.97 (t, $J = 9.0 \text{ Hz}$, 1H), 4.53 (d, $J = 8.0 \text{ Hz}$, 1H), 4.23 (d, $J = 6.0 \text{ Hz}$, 1H), 4.16 (t, $J = 6.0 \text{ Hz}$, 2H), 4.09 (m, 2H), 3.83 (m, 2H), 2.09 (m, 2H), 2.07 (s, 3H), 2.05 (s, 3H), 2.01 (s, 3H), 1.98 (s, 3H). ESIMS m/z 550 ($\text{M} + \text{Na}$)⁺.

3-(2-Aminophenoxy)propyl 2,3,4,6-tetra-O-acetyl- β -D-glucopyranoside (10). A suspension of **9** (360 mg, 0.68 mmol) and 10% Pd-C (50 mg) in EtOAc (50 mL) was stirred in H₂ atmosphere for 2 h and then filtered on a Celite Pad. After the solvent removal, compound **10** was obtained as brown oil (290 mg, 85% yield). IR (KBr): 3441, 2960, 2893, 1755, 1622, 1507, 1368, 1225, 1166, 1041, 908, 750, 613 cm^{-1} . ¹H NMR (300 MHz, CDCl_3) δ 7.82 (d, $J = 9.0 \text{ Hz}$, 1H), 7.52 (t, $J = 7.5 \text{ Hz}$, 1H), 6.76 (m, 4H), 5.19 (t, $J = 9.0 \text{ Hz}$, 1H), 5.08 (t, $J = 9.0 \text{ Hz}$, 1H), 5.00 (t, $J = 9.0 \text{ Hz}$, 1H), 4.52 (d, $J = 8.0 \text{ Hz}$, 1H), 4.26 (d, $J = 6.0 \text{ Hz}$, 1H), 4.13 (m, 2H), 4.08 (m, 2H), 3.85 (m, 2H), 2.09 (m, 2H), 2.08 (s, 3H), 2.02 (s, 3H), 2.00 (s, 3H), 1.99 (s, 3H). ESIMS m/z 520 ($\text{M} + \text{Na}$)⁺.

N-(2-[3-[(2,3,4,6-Tetra-*O*-acetyl- β -*D*-glucopyranosyl)oxy]propoxy]phenyl)piperidine-4-carboxamide (**12**). HOBt (165 mg, 1.21 mmol) and DCC (250 mg, 1.21 mmol) were added to a solution of 1-(*t*-butoxycarbonyl)piperidine-4-carboxylic acid (280 mg, 1.21 mmol) in dry DCM (15 mL). Compound **10** (600 mg, 1.21 mmol) was added after 30 min of stirring, and the reaction mixture was further stirred at room temperature for 48 h. DCU was removed by filtration, and the filtrate was concentrated under reduced pressure. The oily residue was dissolved in EtOAc (50 mL) and sequentially washed twice with saturated 10% Na₂CO₃, 2 N HCl, and brine. The organic phase was dried (Na₂SO₄), filtered, and concentrated under reduced pressure to provide the *N*-Boc-protected compound **11** as an oil (600 mg, 70% yield). After removal of the Boc protecting group with redistilled TFA (21 mL) in CHCl₃ (10 mL), the TFA salt **12** was obtained as brown oil. The oil residue was suspended in water (30 mL), and 2 N NaOH was added to alkaline pH. The aqueous suspension was then extracted with EtOAc (3 × 30 mL), and the combined organic layers were dried (Na₂SO₄) and concentrated under reduced pressure to afford **12** free base as pale-brown oil (420 mg, 80% yield), which was used in the next reaction without further purification. IR (KBr) 3430, 1750, 1625, 1220, 1168, 1041, 750, 613 cm⁻¹. ¹H NMR (300 MHz, DMSO-*d*₆) δ 10.05 (s, 1H), 7.85 (d, *J* = 9.0 Hz, 1H), 7.50 (t, *J* = 7.5 Hz, 1H), 6.77 (m, 2H), 5.21 (t, *J* = 9.0 Hz, 1H), 5.12 (t, *J* = 9.0 Hz, 1H), 5.05 (t, *J* = 9.0 Hz, 1H), 4.55 (d, *J* = 8.0 Hz, 1H), 4.26 (d, *J* = 6.0 Hz, 1H), 4.15–4.10 (m, 2H), 4.08–4.00 (m, 2H), 3.90–3.85 (m, 2H), 3.50–3.30 (m, 2H), 3.25–3.15 (m, 2H), 2.65–2.50 (m, 1H), 2.15–2.08 (m, 2H), 2.08 (s, 3H), 2.02 (s, 3H), 2.00 (s, 3H), 1.99 (s, 3H), 1.90–1.80 (m, 2H), 1.75–1.60 (m, 2H). ESIMS *m/z* 631 (M + Na)⁺.

1-Isopropyl-*N*-(2-[3-[(2,3,4,6-tetra-*O*-acetyl- β -*D*-glucopyranosyl)oxy]propoxy]phenyl)piperidine-4-carboxamide (**13**). Na(CN)BH₃ (100 mg, 1.77 mmol) and 1.25 M HCl solution in MeOH (1 mL) were added to a 0 °C solution of **12** (400 mg, 0.82 mmol) in Me₂CO (5 mL) and MeOH (15 mL), and the mixture was stirred 1 h at 0 °C and overnight at room temperature. After the solvent removal, the residue was dissolved in EtOAc (50 mL), and the organic phase was washed twice with brine, dried (Na₂SO₄), filtered, and concentrated. The residue was purified by flash chromatography (mobile phase DCM/MeOH, 95:5 v/v) to afford **13** as brown oil (215 mg, 50% yield). IR (KBr) 3320, 1748, 1625, 1225, 1040, 750, 613 cm⁻¹. ¹H NMR (300 MHz, DMSO-*d*₆) δ 10.05 (s, 1H), 7.85 (d, *J* = 9.0 Hz, 1H), 7.50 (t, *J* = 7.5 Hz, 1H), 6.77 (m, 2H), 5.21 (t, *J* = 9.0 Hz, 1H), 5.12 (t, *J* = 9.0 Hz, 1H), 5.05 (t, *J* = 9.0 Hz, 1H), 4.55 (d, *J* = 8.0 Hz, 1H), 4.26 (d, *J* = 6.0 Hz, 1H), 4.15–4.10 (m, 2H), 4.08–4.00 (m, 2H), 3.90–3.85 (m, 2H), 3.50–3.30 (m, 2H), 3.25–3.15 (m, 2H), 3.15–3.05 (m, 1H), 2.65–2.50 (m, 1H), 2.15–2.08 (m, 2H), 2.08 (s, 3H), 2.02 (s, 3H), 2.00 (s, 3H), 1.99 (s, 3H), 1.90–1.80 (m, 2H), 1.75–1.60 (m, 2H), 1.26 (d, *J* = 6.5 Hz, 6H). ESIMS *m/z* 673 (M + Na)⁺.

N-(2-[3-(β -*D*-Glucopyranosyloxy)propoxy]phenyl)-1-isopropylpiperidine-4-carboxamide (**14**). MeONa (100 mg, 1.85 mmol) was added to a 0 °C solution of **13** (200 mg, 0.31 mmol) in MeOH (10 mL), and the mixture was stirred overnight at room temperature. After concentration under reduced pressure, the solid residue was purified by silica gel flash chromatography (mobile phase DCM/MeOH, 95:5 v/v), providing **14** as white solid (110 mg, 70% yield), mp 134–136 °C. IR (KBr) 3325, 1650, 1260, 1040, 750 cm⁻¹. ¹H NMR (300 MHz, DMSO-*d*₆) δ 9.95 (s, 1H), 7.82 (d, *J* = 9.0 Hz, 1H), 7.51 (t, *J* = 7.5 Hz, 1H), 6.80–6.75 (m, 2H), 5.19 (t, *J* = 9.0 Hz, 1H), 5.10 (t, *J* = 9.0 Hz, 1H), 5.05 (t, *J* = 9.0 Hz, 1H), 4.90 (s br, 4H), 4.55 (d, *J* = 8.0 Hz, 1H), 4.25 (d, *J* = 6.0 Hz, 1H), 4.15–4.10 (m, 2H), 4.10–4.00 (m, 2H), 3.90–3.85 (m, 2H), 3.50–3.30 (m, 2H), 3.25–3.15 (m, 2H), 3.15–3.05 (m, 1H), 2.65–2.50 (m, 1H), 2.15–2.08 (m, 2H), 1.85–1.70 (m, 2H), 1.65–1.50 (m, 2H), 1.10 (d, *J* = 6.5 Hz, 6H). ESIMS *m/z* 505 (M + Na)⁺. HRMS (ESI) calcd for C₂₄H₃₈N₂O₈ ([M + H]⁺) 483.2701; found 483.2597. Anal. Calcd for C₂₄H₃₈N₂O₈·2.5H₂O: C, 54.60; H, 8.20; N, 5.31. Found: C, 54.81; H, 7.76; N, 5.40.

Lipophilicity Measurements. The lipophilicity of compounds **1–3** was determined by a reversed-phase (RP) HPLC method, using a Phenomenex Synergi C18 (4.6 mm × 150 mm i.d., 5 μ m particles)

column (Phenomenex Italy, Castel Maggiore, BO, Italy) as the nonpolar stationary phase, and retention data were measured at regular increments of the volume fraction of MeOH in pH 4.5 phosphate buffer (0.05 M). All the RP-HPLC measurements were carried out at temperature of 25 ± 0.2 °C, flow-rate of 1.0 mL min⁻¹ and UV detection at 288 nm wavelength, using a Waters HPLC 1525 multisolvent delivery system equipped with a Waters 2487 variable wavelength UV detector (Waters Assoc., Milford, MA, USA). Capacity factors (*k'*) of each compound at different mobile phase compositions (0.05 increments of the MeOH volume fraction, ϕ , ranging between 0.8 and 0.4) were calculated as $k' = (t_R - t_0)/t_0$, where t_R is the retention time of the solute and t_0 is the column dead time, measured as the solvent front. The log *k'* values increased linearly ($r^2 > 0.95$) with decreasing ϕ . Linear regression analysis was performed on at least five data points (the lowest MeOH volume fractions) for each compound and the linear relationship extrapolated to 100% aqueous mobile phase to yield log *k'*_w value.

Aqueous Solubility. The aqueous solubility of compounds **1–3** was determined at pH 7.4 in a 0.05 M phosphate buffer (containing 0.15 M KCl as ionic strength regulator) in deionized water. An excess of each compound (4–10 mg) was added to 1 mL of buffered solution, and the suspension was shaken 1 h at 25 °C. The suspension was then maintained for 15 min at the same temperature and without shake, to ensure the solubility equilibrium. Subsequently, the supernatant was filtered (Millipore 0.45 μ m), and the solution was analyzed by HPLC. Analyses were performed on a Phenomenex Gemini C18 column (5 μ m, 150 mm × 4.6 mm i.d.) using MeOH and 0.05 M phosphate buffer solution (pH 4.5) mixed in different fraction composition depending upon the retention of the analyte as the mobile phase (flow rate 1 mL·min⁻¹; detection at 288 nm). Calibration curves were obtained by measuring peak areas for each compound at known concentrations.

Stability in Water and Human Plasma. Stability of compounds **1–3** was determined either in phosphate buffer solution (pH 7.4) and human plasma at 37 °C. For each compound, the stock solution in ACN (10 mM) was diluted to a final incubation concentration of 250 μ M. The incubation at 37 °C was stopped at 1, 2, and 4 h and the samples treated and analyzed by HPLC using the above analytical conditions.

For the stability study in the aqueous medium, the stock solution (0.25 mL) was added to 9.75 mL of 0.05 M phosphate buffer solution at pH 7.40 (0.15 M KCl as ionic strength regulator). At t_0 and each other fixed time, a solution sample (0.5 mL) was withdrawn, filtered (Millipore 0.45 μ m), and analyzed by HPLC. For the stability measurements in human plasma, the stock solution (0.037 mL) was added to 1.463 mL of preheated (37 °C) human serum (lyophilized and reconstituted with 4 mL of deionized water). The incubation at 37 °C was stopped at each fixed time by adding 0.4 mL of ice-cold ACN to 0.2 mL of serum solution. The sample was vortexed for 1 min and then centrifuged for 10 min at 3500 rcf before HPLC injection of the supernatant. The percentage of the remaining test compound was measured by monitoring the peak area of the chromatogram.

Crystallization of Human Thrombin with Inhibitors **2 and **3**.** Human α -thrombin supplied in 50% (v/v) glycerol/H₂O solution and hirugen peptide (exosite inhibitor having sequence Ac-NGDFEETPEEY(SO₃⁻)L) used for crystallization experiments were purchased from Haematologic Technologies Inc. (Essex Junction, VT, USA) and GL Biochem (Shanghai), respectively. To avoid the fast autolysis of thrombin during crystallization, a 0.25 mM solution containing protein was preliminarily incubated in the presence of 2.5 mM hirugen peptide for 4 h at 20 °C. The resulting thrombin–hirugen adduct solution was centrifuged (10,000 rpm at 4 °C) by using Amicon Ultra centrifuge filter having a cut off of 10 kDa (Millipore Corporation) to exchange the starting buffer containing glycerol with a solution containing 20 mM HEPES pH 7.1, 750 mM NaCl, and 0.1 mM hirugen. At the end of buffer exchange, the protein–hirugen adduct was concentrated up to 13 mg·mL⁻¹. Large lanceolate crystals (100–200 μ m) of thrombin–hirugen complex were grown in 1 week as described by Skrzypczak-Jankun et al.³⁰ a drop having volume of 2 μ L, formed by 1 μ L of solution containing 12–13 mg·mL⁻¹ of

protein–hirugen adduct and 1 μL of reservoir solution, containing 28–30% PEG4000, 100 mM HEPES, pH 7.0, and 0.04% NaN_3 , was equilibrated against 1 mL of reservoir solution. Crystallization experiments were performed in vapor diffusion, hanging drop setup, at 20 °C. Thrombin–hirugen crystals were stabilized for 5 min in a solution containing 30.9% PEG4000, 100 mM HEPES, pH 7.0, and 0.04% NaN_3 and soaked for 3 days in a solution with the same composition plus 43 mM compound 3 or 100% satd 2. In both cases, the soaking solution contained 20% (v/v) DMSO to facilitate the solubilization of the inhibitor molecule.

Data Collection, Structure Solution, and Refinement.

Diffraction data for thrombin–3 adduct were collected by using a home diffractometer equipped by a Rigaku R-axis-IIc imaging plate system, with Cu $K\alpha$ radiation (IBB-CNR, Napoli, IT), whereas diffraction data for thrombin–2 adduct were collected at the beamline I0–04 of the Diamond Light Source (Oxford, UK) by using a radiation wavelength of 0.978 Å. The oscillation angle was set to 1° for each data collection, while the sample–detector distance was chosen according to the diffraction data resolution. Data reduction was performed by using the XDS program,³¹ while POINTLESS and SCALA³² were used to define the space group and to scale the intensity of the reflections, respectively. The molecular replacement (MR) program REMO,³³ included into ILMILIONE,³⁴ was employed for phasing. The Protein Data Bank (PDB) file 1HGT,³¹ having 100% of homology sequence with the protein used in the crystallization experiments, was used as search model. For both crystals, the MR solution was improved by using Phenix.Autobuild wizard (PHENIX package)³⁵ in the “rebuild-in-place” mode. The COOT software³⁶ was used to inspect the electron density map and to fit the inhibitor molecules 2 and 3, whose addition resulted in a decrease of the R and R_{free} values. The protein–ligand adduct structures were refined by using Phenix.refine³⁷ (PHENIX package) and validated by MolProbity.³⁸ Their atomic coordinates and structure factors have been deposited in the RCSB PDB under the accession codes 4NZE and 4N3L for the thrombin–2 and –3 adducts, respectively. Information on unit cell and refinement parameters for each structure are summarized in Table 3.

Inhibition Assays of Factor Xa and Thrombin. The test compounds were assayed in vitro for their inhibitory activity toward fXa and fIIa, determining the hydrolysis rates of the synthetic chromogenic substrates monitored at 405 nm. Enzymes and substrates were used as follows, in final concentrations: 2 nM human fXa and 0.04 mM S-2765 (*Z*-D-Arg-Gly-Arg-*p*-NA) from Chromogenix AB-Instrumentation Laboratories (Milan, Italy), 0.41 $\text{U}\cdot\text{mL}^{-1}$ bovine thrombin from Sigma-Aldrich (Milan, Italy), and 0.05 mM S-2238 (*D*-Phe-Pip-Arg-*p*-NA) from Chromogenix AB-Instrumentation Laboratories (Milan, Italy). Enzyme solutions were incubated with DMSO solutions of the test inhibitor (DMSO did not exceed 1%) in various concentrations (0.01–100 nM or 0.01–100 μM), before the respective chromogenic substrates added to start the enzyme kinetics. The kinetic studies were performed at pH 8. Reactions were initiated with adding 500 μL of substrate solutions and increase in absorbance monitored for 5 min. The initial velocities were determined and the concentration of the inhibitor required to diminish by 50% the control velocity (IC_{50}), calculated by nonlinear (sigmoid) regression. Three independent IC_{50} values were determined for calculating inhibition constants K_i using the Cheng–Prusoff equation.¹⁵ To determine the type of inhibition for the most potent inhibitor 3 and the parent compound 1, the Lineweaver–Burk eq ($1/v$ vs $1/[S]$) was fitted for varying concentrations of substrates (25–200 μM and 6–400 μM for fXa and fIIa, respectively) in the absence or presence of inhibitor at four different concentrations, using fixed amounts of enzymes (2 nM for fXa and 0.41 $\text{U}\cdot\text{mL}^{-1}$ for fIIa). Replotting the slopes of the above plots against the inhibitor concentration yielded the K_i value as the x -axis intercept (Figure 2).

Anticoagulant Activity. The effect of compounds 1–3 on thrombin generation (TG) in human plasma was evaluated by the calibrated automated thrombography (CAT) as described by Hemker et al.²³ Briefly, 80 μL of human citrated plasma were dispensed into round-bottomed 96-well plates and incubated for 10 min at 37 °C with

5 pmol/L recombinant tissue factor (TF) and procoagulant phospholipids (4 $\mu\text{mol/L}$, MP Reagent). Analysis was performed in a final volume of 120 μL , and started upon addition of 20 μL of a mixture containing 100 mmol/L CaCl_2 and 2.5 mmol/L ZGGR-AMC (Fluca Reagent, Diagnostica Stago, Asnieres, France). Measurements were taken every 20 s in a Fluoroskan Ascent fluorometer (Thermo Fisher Scientific, Waltham, MA, USA) and data were analyzed using the Thrombinoscope software (Diagnostica Stago). The parameters calculated by the software were the lag-time (LT), the thrombin peak (TP), and endogenous thrombin potential (ETP). All samples and calibrators were run at least in duplicate.

Profibrinolytic Activity. The effect of compounds 1–3 on plasma fibrinolysis was investigated by a turbidimetric assay, which evaluates the fibrinolysis time of TF-induced plasma clots exposed to exogenous tissue plasminogen activator (t-PA). The assay was performed as reported^{39,40} with slight modifications. First, 100 μL of plasma, 10 μL of phospholipids (4 $\mu\text{mol/L}$, MP Reagent, Diagnostica Stago), 5 μL of t-PA (40 ng/mL), 20 μL of Tris-NaCl buffer (20 mmol/L Tris-HCl, 150 mmol/L NaCl, pH 7.4), and 5 μL of TF (5 pmol/L) were loaded in microplate wells, after which the clotting reaction was started with 100 μL of CaCl_2 (8.3 mmol/L). The plate was then incubated at 37 °C in a microplate reader (Multiskan FC; Thermo Fisher Scientific), and the changes in optical density measured at 405 nm every minute for 3 h. Clotting time was defined as the time to reach the midpoint of clear-to-maximum turbid transition, whereas clot lysis time was defined as the time from clot formation to the midpoint of the maximum turbid-to-clear transition.

■ ASSOCIATED CONTENT

📄 Supporting Information

Experimental details on synthesis, along with spectral data (IR, NMR, MS) and elemental analyses (C, H, N), of non-glycosylated compounds 5, 6, 7a, 7b, 8a, and 8b. This material is available free of charge via the Internet at <http://pubs.acs.org>.

■ AUTHOR INFORMATION

Corresponding Author

*Phone: +39-080-5442781. Fax: +39-080-5442230. E-mail: cosimodamiano.altomare@uniba.it.

Present Address

¶For G.L.: Drug Design & Discovery, Aptuit, Via A. Fleming, 37135 Verona, Italy.

Author Contributions

M.d.C., G.Z., G.L., and C.D.A. contributed to chemistry and performed enzymes' inhibition measurements. B.D.D. and R.C. carried out crystallographic experiments and data analysis. F.I. and M.C. carried out evaluation of the antithrombotic properties and interpretation of the data. C.D.A. designed the research project and interpreted data. All the authors contributed to write the manuscript.

Notes

The authors declare no competing financial interest.

■ ACKNOWLEDGMENTS

We thank DIAMOND LIGHT LTD synchrotron (Oxford, UK) for beam time, Mr. Giosuè Sorrentino and Mr. Maurizio Amendola for their support during X-ray measurements at the IBB (CNR, Napoli), and Dr. Maria Brunella Aresta for their support in the crystallization experiments. The support of CCNC consortium (Collezione Nazionale di Composti Chimici e Centro Screening) is gratefully acknowledged.

■ ABBREVIATIONS USED

aPTT, activated partial thromboplastin time; ACN, acetonitrile; AF, atrial fibrillation; CAT, calibrated automated thrombography; DCU, dicyclohexylurea; DTI, direct thrombin inhibitor; DVT, deep venous thrombosis; ETP, endogenous thrombin potential; fIIa, thrombin; fXa, activated factor X; hfIIa, human thrombin; HEPES, 2-[4-(2-hydroxyethyl)piperazin-1-yl]ethanesulfonic acid; HOBt, 1-benzotriazole; INR, international normalized ratio; LT, lag time; NOACs, new orally active anticoagulants; PT, prothrombin time; rcf, relative centrifugal force; RP, reversed phase; TF, tissue factor; TG, thrombin generation; t-PA, tissue plasminogen activator; TP, thrombin peak; VKAs, vitamin K antagonists

■ REFERENCES

- (1) Reiffel, J. A. Novel oral anticoagulants. *Am. J. Med.* **2014**, *127*, e16–17.
- (2) Haas, S. New oral Xa and IIa inhibitors: updates on clinical trial results. *J. Thromb. Thrombolysis* **2008**, *25*, 52–60.
- (3) Alban, S. Pharmacological strategies for inhibition of thrombin activity. *Curr. Pharm. Des.* **2008**, *14*, 1152–1175.
- (4) Deitelzweig, S. Practical considerations in the use of novel oral anticoagulants for stroke prevention in nonvalvular atrial fibrillation. *Cardiovasc. Ther.* **2014**, *32*, 74–81.
- (5) Wang, Y.; Bajorek, B. New oral anticoagulants in practice: pharmacological and practical considerations. *Am. J. Cardiovasc. Drugs* **2014**, *14*, 175–189.
- (6) Huel, N. H.; Nar, H.; Priepe, H.; Ries, U.; Stassen, J.-M.; Wiene, W. Structure-based design of novel potent nonpeptide thrombin inhibitors. *J. Med. Chem.* **2002**, *45*, 1757–1766.
- (7) Maignan, S.; Guilloleau, J. P.; Pouzieux, S.; Choi-Sledeski, Y. M.; Becker, M. R.; Klein, S. I.; Ewing, W. R.; Pauls, H. W.; Spada, A. P.; Mikol, V. Crystal structures of human factor Xa complexed with potent inhibitors. *J. Med. Chem.* **2000**, *43*, 3226–3232.
- (8) de Candia, M.; Lopopolo, G.; Altomare, C. Novel factor Xa inhibitors: a patent review. *Expert Opin. Ther. Pat.* **2009**, *19*, 1535–1580.
- (9) de Candia, M.; Liantonio, F.; Carotti, A.; De Cristofaro, R.; Altomare, C. Fluorinated benzyloxyphenyl piperidine-4-carboxamides with dual function against thrombosis: inhibitors of factor Xa and platelet aggregation. *J. Med. Chem.* **2009**, *52*, 1018–1028.
- (10) Lopopolo, G.; Fiorella, F.; de Candia, M.; Nicolotti, O.; Martel, S.; Carrupt, P.-A.; Altomare, C. Biaryl-methoxy isonipecotanilides as potent and selective inhibitors of blood coagulation factor Xa. *Eur. J. Pharm. Sci.* **2011**, *42*, 180–191.
- (11) de Candia, M.; Fiorella, F.; Lopopolo, G.; Carotti, A.; Romano, M. R.; Lograno, M. D.; Martel, S.; Carrupt, P. A.; Belviso, B. D.; Caliandro, R.; Altomare, C. Synthesis and biological evaluation of direct thrombin inhibitors bearing 4-(piperidin-1-yl)pyridine at the P1 position with potent anticoagulant activity. *J. Med. Chem.* **2013**, *56*, 8696–8711.
- (12) Lopopolo, G.; de Candia, M.; Panza, L.; Romano, M. R.; Lograno, M. D.; Campagna, F.; Altomare, C. β -D-Glucosyl conjugates of highly potent inhibitors of blood coagulation factor Xa bearing 2-chlorothiophene as a P1 motif. *ChemMedChem* **2012**, *7*, 1669–1677.
- (13) Nazaré, M.; Will, D. W.; Matter, H.; Schreuder, H.; Ritter, K.; Urmann, M.; Essrich, M.; Bauer, A.; Wagner, M.; Czech, J.; Lorenz, M.; Laux, V.; Wehner, V. Probing the subpockets of factor Xa reveals two binding modes for inhibitors based on a 2-carboxyindole scaffold: a study combining structure–activity relationship and X-ray crystallography. *J. Med. Chem.* **2005**, *48*, 4511–4525.
- (14) Salonen, L. M.; Bucher, C.; Banner, D. W.; Haap, W.; Mary, J.-L.; Benz, J.; Kuster, O.; Seiler, P.; Schweizer, W. B.; Diederich, F. Cation- π interactions at the active site of factor Xa: dramatic enhancement upon stepwise N-alkylation of ammonium ions. *Angew. Chem., Int. Ed.* **2009**, *48*, 811–814.
- (15) Cheng, Y.; Prusoff, W. H. Relation between the inhibition constant (K_i) and the concentration of inhibitor which causes fifty per cent inhibition (I_{50}) of an enzymic reaction. *Biochem. Pharmacol.* **1973**, *22*, 3099–3108.
- (16) Skrzypczak-Jankun, E.; Carperos, V. E.; Ravichandran, K. G.; Tulinsky, A.; Westbrook, M.; Maraganore, J. M. Structure of the hirugen and hirulog 1 complexes of α -thrombin. *J. Mol. Biol.* **1991**, *221*, 1379–1393.
- (17) Imai, Y. N.; Inoue, Y.; Nakanishi, I.; Kitauro, K. Cl– π interactions in protein–ligand complexes. *Protein Sci.* **2008**, *17*, 1129–1137.
- (18) Di Cera, E.; Dang, Q. D.; Ayala, Y. M. Molecular mechanisms of thrombin function. *Cell. Mol. Life Sci.* **1997**, *53*, 701–730.
- (19) Dang, Q. D.; Vindigni, A.; Di Cera, E. An allosteric switch controls the procoagulant and anticoagulant activities of thrombin. *Proc. Natl. Acad. Sci. U. S. A.* **1995**, *92*, 5977–5981.
- (20) Banfield, D. K.; MacGillivray, R. T. A. Partial characterization of vertebrate prothrombin cDNAs: amplification and sequence analysis of the B chain of thrombin from nine different species. *Proc. Natl. Acad. Sci. U. S. A.* **1992**, *89*, 2779–2783.
- (21) Zhang, E.; Tulinsky, A. The molecular environment of the Na⁺ binding site of thrombin. *Biophys. Chem.* **1997**, *63*, 185–200.
- (22) Huntington, J. A. How Na⁺ activates thrombin—a review of the functional and structural data. *Biol. Chem.* **2008**, *389*, 1025–1035.
- (23) Hemker, H. C.; Al Dieri, R.; De Smedt, E.; Béguin, S. Thrombin generation, a function test of the haemostatic–thrombotic system. *Thromb. Haemostasis* **2006**, *96*, 553–561.
- (24) Samama, M. M.; Le Flem, L.; Guinet, C.; Gerotziakas, G.; Depasse, F. Three different patterns of calibrated automated thrombogram obtained with six different anticoagulants. *J. Thromb. Haemostasis* **2007**, *5*, 2554–2556.
- (25) Colucci, M.; Semeraro, N. Thrombin activatable fibrinolysis inhibitor: at the nexus of fibrinolysis and inflammation. *Thromb. Res.* **2012**, *129*, 314–9.
- (26) Bouma, B. N.; Mosnier, L. O. Thrombin activatable fibrinolysis inhibitor (TAFI)—how does thrombin regulate fibrinolysis? *Ann. Med.* **2006**, *38*, 378–388.
- (27) Lisman, T.; Adelmeijer, J.; Nieuwenhuis, H. K.; de Groot, P. G. Enhancement of fibrinolytic potential in vitro by anticoagulant drugs targeting activated factor X, but not by those inhibiting thrombin or tissue factor. *Blood Coagulation Fibrinolysis* **2003**, *14*, 557–562.
- (28) Ammollo, C. T.; Semeraro, F.; Semeraro, N.; Colucci, M. The contribution of anti-Xa and anti-IIa activities to the profibrinolytic activity of low-molecular-weight heparins. *Thromb Haemostasis* **2009**, *101*, 782–785.
- (29) Turpie, A. G. G. Oral, direct factor Xa inhibitors in development for the prevention and treatment of thromboembolic diseases. *Arterioscler. Thromb. Vasc. Biol.* **2007**, *27*, 1238–1247.
- (30) Wong, P. C.; Pinto, D. J. P.; Zhang, D. Preclinical discovery of apixaban, a direct and orally bioavailable factor Xa inhibitor. *J. Thromb. Thrombolysis* **2011**, *31*, 478–492.
- (31) Skrzypczak-Jankun, E.; Carperos, V. E.; Ravichandran, K. G.; Tulinsky, A.; Westbrook, M.; Maraganore, J. M. Structure of the hirugen and hirulog 1 complexes of α -thrombin. *J. Mol. Biol.* **1991**, *221*, 1379–1393.
- (32) Kabsch, W. XDS. *Acta Crystallogr., Sect. D: Biol. Crystallogr.* **2010**, *D66*, 125–132.
- (33) Evans, P. R. Scaling and assessment of data quality. *Acta Crystallogr., Sect. D: Biol. Crystallogr.* **2006**, *D62*, 72–82.
- (34) Caliandro, R.; Carrozzini, B.; Cascarano, G. L.; De Caro, L.; Giacobozzo, C.; Mazzone, A.; Siliqi, D. Molecular replacement: the approach of the program REMO. *J. Appl. Crystallogr.* **2006**, *39*, 185–193.
- (35) Burla, M. C.; Caliandro, R.; Camalli, M.; Carrozzini, B.; Cascarano, G. L.; De Caro, L.; Giacobozzo, C.; Polidori, G.; Siliqi, D.; Spagna, R. IL MILIONE: a suite of computer programs for crystal structure solution of proteins. *J. Appl. Crystallogr.* **2007**, *40*, 609–613.
- (36) Adams, P. D.; Afonine, P. V.; Bunkóczi, G.; Chen, V. B.; Davis, I. W.; Echols, N.; Headd, J. J.; Hung, L.-W.; Kapral, R. W.; Grosse-

Kunstleve, A. J.; McCoy, N. W.; Moriarty, R.; Oeffner, R. J.; Read, D. C.; Richardson, J. S.; Richardson, G. J.; Terwilliger, T. C.; Zwart, P. H. PHENIX: a comprehensive Python-based system for macromolecular structure solution. *Acta Crystallogr., Sect. D: Biol. Crystallogr.* **2010**, *D66*, 213–221.

(37) Emsley, P.; Cowtan, K. COOT: model-building tools for molecular graphics. *Acta Crystallogr., Sect. D: Biol. Crystallogr.* **2004**, *D60*, 2126–2132.

(38) Afonine, P. V.; Grosse-Kunstleve, R. W.; Echols, N.; Headd, J. J.; Moriarty, N. W.; Mustyakimov, M.; Terwilliger, T. C.; Urzhumtsev, A.; Zwart, P. H.; Adams, P. D. Towards automated crystallographic structure refinement with phenix.refine. *Acta Crystallogr., Sect. D: Biol. Crystallogr.* **2012**, *D68*, 352–367.

(39) Chen, V. B.; Arendall, W. B., III; Headd, J. J.; Keedy, D. A.; Immormino, R. M.; Kapral, G. J.; Murray, L. W.; Richardson, J. S.; Richardson, D. C. MolProbity: all-atom structure validation for macromolecular crystallography. *Acta Crystallogr., Sect. D: Biol. Crystallogr.* **2010**, *D66*, 12–21.

(40) Colucci, M.; Binetti, B. M.; Tripodi, A.; Chantarangkul, V.; Semeraro, N. Hyperprothrombinemia associated with prothrombin G20210A mutation inhibits plasma fibrinolysis through a TAFI-mediated mechanism. *Blood* **2004**, *103*, 2157–2161.